Multispectral *in vivo* three-dimensional optical coherence tomography of human skin

Aneesh Alex
Cardiff University
School of Optometry and Vision Sciences
Biomedical Imaging Group
Cardiff, Wales, United Kingdom

Boris Považay
Bernd Hofer
Medical University Vienna
Center for Medical Physics and Biomedical Engineering
Währinger Gürtel 18-20
Vienna, 1090 Austria
and
Cardiff University
School of Optometry and Vision Sciences
Biomedical Imaging Group
Cardiff, Wales, United Kingdom

Sergei Popov
Imperial College
Department of Physics
London, SW7 2AZ United Kingdom

Carl Glittenberg
Susanne Binder
Ludwig Boltzmann Institute
Department of Ophthalmology
Rudolf Foundation Clinic Vienna
Juchgasse 25
Vienna, 1030 Austria

Wolfgang Drexler
Medical University Vienna
Center for Medical Physics and Biomedical Engineering
Währinger Gürtel 18-20
Vienna, 1090 Austria
and
Cardiff University
School of Optometry and Vision Sciences
Biomedical Imaging Group
Cardiff, Wales, United Kingdom

Abstract. The capability of optical coherence tomography (OCT) to perform "optical biopsy" of tissues within a depth range of 1 to 2 mm with micron-scale resolution in real time makes it a promising biomedical imaging modality for dermatologic applications. Three high-speed, spectrometer-based frequency-domain OCT systems operating at 800 nm (20,000 A-scans/s), 1060 nm, and 1300 nm (both 47,000 A-scans/s) at comparable signal-to-noise ratio (SNR), SNR roll-off with scanning depth, and transverse resolution (<15 μm) were used to acquire 3-D tomograms of glabrous and hairy human skin *in vivo*. Images obtained using these three systems were compared in terms of penetration depth, resolution, and contrast. Normal as well as abnormal sites like moles and scar tissue were examined. In this preliminary study, skin pigmentation had little effect on penetration accomplished at three different wavelengths. The epidermis and dermal–epidermal junction could be properly delineated using OCT at 800 nm, and this wavelength offered better contrast over the other two wavelength regions. OCT at 1300 nm permits imaging of deeper dermal layers, critical for detecting deeper tumor boundaries and other deeper skin pathologies. The performance at 1060 nm compromises between the other wavelengths in terms of penetration depth and image contrast.
© 2010 Society of Photo-Optical Instrumentation Engineers. [DOI: 10.1117/1.3400665]

Keywords: coherent optical systems; imaging systems; tomography; three dimensions; lasers in medicine; fiber optics.

Paper 09509R received Nov. 17, 2009; revised manuscript received Feb. 16, 2010; accepted for publication Mar. 4, 2010; published online May 4, 2010.

1 Introduction

Optical coherence tomography (OCT) is a noninvasive *in vivo* biomedical imaging modality capable of generating three-dimensional (3-D) images of tissue microstructure.[1–3] To date, OCT has had the largest clinical impact in ophthalmology.[4] In the past decade, development of ultra-broadband light sources,[5,6] advances in fiber optics, and introduction of frequency-domain techniques[7] have provided significant improvements in resolution,[8] detection sensitivity,[9–11] and image acquisition speed.[12,13] In most of the biological tissues such as skin, the major limiting factor of OCT is its penetration depth due to strong scattering and absorption of light. However, this imaging depth of around 1 to 2 mm is comparable to the depth at which many biopsies are performed. In addition, many diagnostically important changes in tissue morphology, such as those associated with malignant conditions[14] and various cutaneous diseases,[15,16] occur in epithelial tissues. The capability of OCT to perform "optical biopsy" *in situ* in real time with unprecedented resolution makes it a promising noninvasive imaging modality for visualization and interpretation of microstructural information of different types of tissues.

Address all correspondence to: Wolfgang Drexler, Medical University Vienna, Center for Medical Physics and Biomedical Engineering, Währinger Gürtel 18-20, Vienna, 1090 Austria. Tel: 43-1-40400-1984; Fax: 43-1-40400-3988; E-mail: wolfgang.drexler@meduniwien.ac.at

1083-3668/2010/15(2)/026025/15/$25.00 © 2010 SPIE

Table 1 Specifications of three OCT systems. Two alternative light sources were used for 1300-nm imaging.

		Ti:sapphire	Amplified spontaneous emission	Yb-doped fiber laser	Super luminescent diode
Central wavelength	nm	800	1050	1250	1320
Bandwidth	nm	140	72	140	100
Axial resolution	μm	~3	~7	~6	~7
Transverse	μm	~12	~12	~15	~15
Imaging speed	kHz	20	47	47	47
Signal-to-noise ratio	dB	91	93	94	94
Power on sample	mW	4	3	2.5	2.5

Excisional biopsy and histology represent the "gold standard" for morphological investigation of biological tissues. The ultimate aim of noninvasive *in vivo* biomedical imaging modalities is to access the three-dimensional morphology of macroscopic volumes of thick areas ($>10\times10$ mm^2), with a resolution similar to that of histology at speeds compatible to clinical requirements, i.e., within seconds or even real time, to reduce motion artifacts. In dermatology, several imaging methodologies including epiluminescence microscopy (ELM),[17–19] confocal laser microscopy (CLM),[20–23] high-frequency ultrasound imaging (HFUS),[24–26] multiphoton tomography (MPT),[27–29] magnetic resonance imaging (MRI),[30–32] and OCT are being employed and investigated to realize this goal. Since its introduction into dermatology in 1997, OCT has been utilized to obtain qualitative and quantitative information from human skin *in vivo*.[33–37] Polarization-sensitive[38–40] and flow-sensitive[41] approaches have been incorporated into many OCT systems, allowing complementary functional information and increased contrast to be obtained alongside the structural OCT images.[42] In addition to visualization of micromorphological details, dermal OCT has been used for applications such as detection of skin tumors[14,38,43–45] and various pathologies,[46,47] analysis of inflammatory skin conditions,[15,16] evaluation of treatment effects,[48–50] assessment of burn depth,[39] and monitoring of the wound healing process.[51]

Most OCT systems operate in the wavelength region of 700 to 1300 nm, known as the "optical diagnostic window," where light absorption by tissue components such as water, melanin, and hemoglobin is relatively low. Meanwhile, the majority of OCT systems used for dermal imaging employ the 1300-nm wavelength region. However, due to the variation in tissue optical properties with wavelength, imaging parameters such as resolution, penetration depth, and contrast depend on the central wavelength and bandwidth of the light source. Sainter et al.[52] quantified the appropriateness of common OCT sources based on light–tissue interactions during its propagation through tissues with known optical properties and postulated that higher wavelength sources centered at 1300 nm would be capable of imaging deeper than those centered close to 800 nm. Many comparative studies of OCT at different wavelength regions between 800 nm and 1800 nm have been performed to find an optimum wavelength region for dermal imaging.[53–55] Recently, simultaneous detection of OCT images using two wavelength bands supplied by a single supercontinuum light source have been implemented, both in time and spectral domains.[56,57]

However, owing to variations in experimental conditions or due to differences in the purpose of study, no definite conclusions as to the optimum wavelength region employable for dermal OCT have been reached. Hence, this paper aims for a systematic investigation comparing images of human skin obtained *in vivo* from different locations at three different wavelength regions, each optimized to be similar in terms of SNR, SNR roll-off with depth, and transverse resolution.

2 Materials and Methods

2.1 *Subjects*

During the course of this study, *in vivo* 3-D OCT images of different dermal sites such as skin above the proximal interphalangeal (PIP) joint of the middle finger and dorsal forearm were obtained from three subjects. As suggested by previous studies,[48] contact gel was topically applied to all these imaging sites as an index matching medium to decrease the superficial surface reflectivity, and a tilted glass plate was placed above to avoid specular reflections. To determine the effect of skin pigmentation on OCT, normal subjects comprising skin types II (Caucasian), IV (Indian), and VI (African) according to the Fitzpatrick scale[58] participated in this study. In addition, OCT images of pigmented moles and scar tissue were obtained from two of these volunteers for analysis of the microstructural deformations in these tissues and also to observe the wavelength-dependent variations in visualization of minute morphological details.

2.2 *OCT Systems*

Three spectrometer-based frequency-domain OCT systems operating at 800-nm, 1060-nm, and 1300-nm wavelength regions, respectively, were used to obtain images of human skin

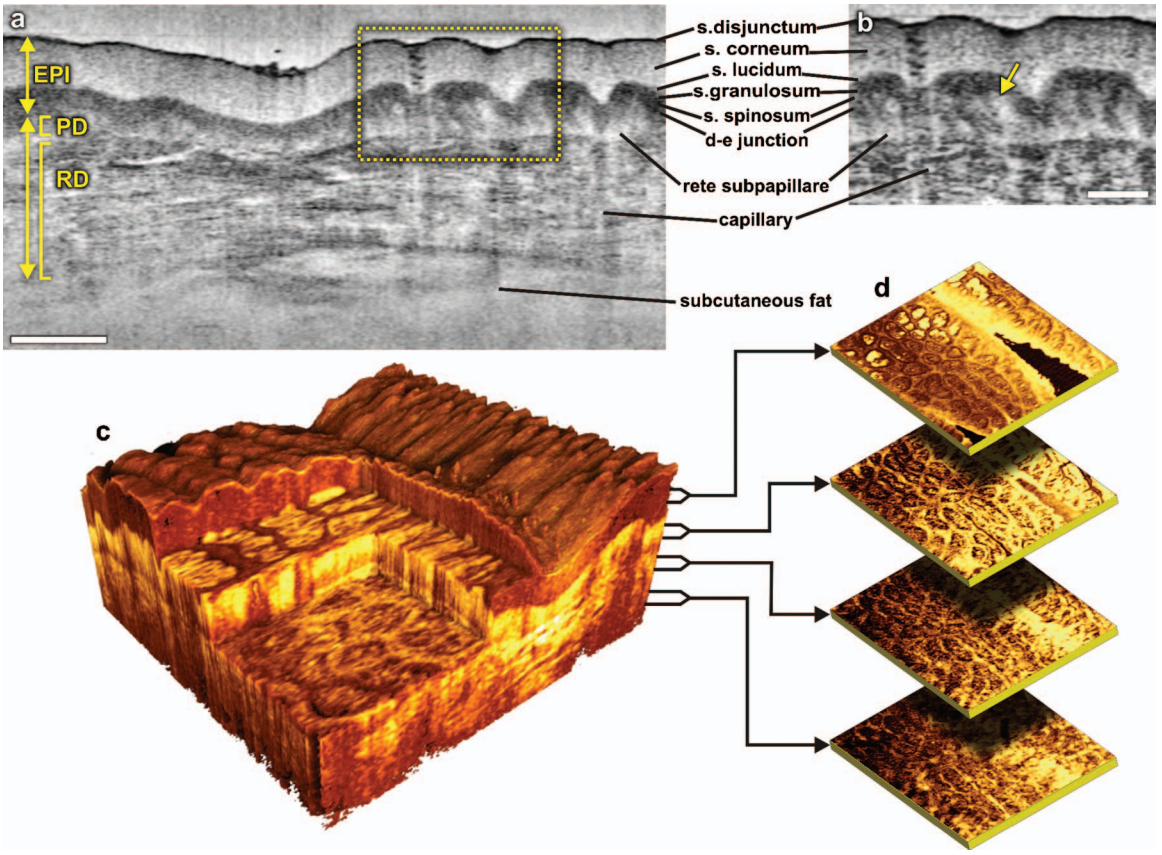

Fig. 1 Different ways to display micromorphological information obtained using OCT. (a) B-scan of skin above the proximal interphalangeal joint of the middle finger obtained using 1300-nm system. (b) Magnified view of different sublayers of epidermis and dermis. The yellow arrow points toward the dermal–epidermal junction. (c) 3-D rendering of the same region reconstructed using 1024 B-scans. (d) *En face* sections of the same region separated in depth by 360 μm. The scale bar in (a) denotes 500 μm, and the scale bar in (b) denotes 200 μm.

in vivo. An ultra-broadband coherent light source ($Ti:Al_2O_3$ laser) was used in the 800-nm OCT system;[5] an amplified spontaneous emission (ASE) source (NP Photonics, Tucson, Arizona) was used in the 1060-nm OCT system; and a ytterbium (Yb)-doped fiber laser[59] and a superluminescent light emitting diode source (Thorlabs, Inc., Newton, New Jersey) were used in the 1300-nm OCT system. A comparison of the main specifications of these OCT systems is given in Table 1.

The design and implementation of these spectrometer-based OCT systems was previously described in detail.[60] Briefly, in all three fiber-based OCT systems, a fiber-optic coupler with an asymmetric splitting ratio was used to divide the light from the source into the sample and reference arms. The reference arm consisted of a free-space pathway with dispersion compensation material for balancing dispersion due to fiber length mismatch and biological tissues, while the sample arm consisted of a handheld probe with two galvanometric mirrors for scanning in two dimensions. The design of the all-reflective spectrometers was based on the Czerny-Turner configuration, which operated in a very compact geometry, maximizing mechanical stability and minimizing internal chromatic aberrations. The digital data were transferred from the respective Si or InGaAs line scan camera to a frame grabber (National Instruments) by a standard CameraLink connection. The timing of the image acquisition and the galvanometric scanners in the sample arm was synchronized by employing a field programmable gate array (National Instruments). Communications between these components of image acquisition hardware were regulated by a LabView programming interface (National Instruments). Typical surface dimensions of a scan region were approximately 8×8 mm^2, with 1024 transverse sampling points per B-scan. Sampling density was set to be just over the critical sampling limit. The wavelength-dependent components of the handheld probe such as the collimator and objective lens were selected appropriately for each system, so that they were comparable in terms of transverse resolution and depth of focus. All three OCT systems were found to be similar in terms of SNR, transverse resolution, and sensitivity roll-off. However, the free-space axial resolution of the 800-nm system was measured to be better than the other two systems (Table 1). Images obtained from approximately the same locations were compared in terms of resolution, contrast, penetration depth, and dynamic range.

3 Results and Discussion

All three OCT systems, with image acquisition rates of 20,000 A-scans/s (800-nm system) and 47,000 A-scans/s (both the 1060-nm and 1300-nm systems), demonstrated the tremendous potential of OCT to manifest micromorphological information about human skin *in vivo*. Figure 1 depicts the capa-

bility of OCT to display the extracted information as cross-sectional images in orthogonal planes [Figs. 1(a) and 1(d)] and in three dimensions [Fig. 1(c)]. The 1300-nm system employing the fiber laser–based source could clearly visualize the morphology of several cutaneous layers such as epidermis, dermis, and even the deeper layer of subcutaneous fat at the palmar side of the PIP joint of the middle finger. Glabrous skin, as found on the palm, allows better discrimination of different layers in the OCT tomogram, and their intensity pattern can be correlated to various anatomical structures. All major cutaneous layers, including different sublayers [Fig. 1(a) and 1(b)], were well delineated due to pronounced differences in scattering. Above the thick and almost transparent *stratum corneum* (SC), the *stratum disjunctum* can be clearly seen as a narrow region with increased scattering, caused by the mix of exfoliated corneal material and air. Higher concentration of eleidin and the lack of intercellular bodies make the *stratum lucidum* a homogenous, even less scattering layer between the *stratum corneum* and *stratum granulosum*. As indicated by the yellow arrow in Fig. 1(b), beneath the highly reflecting *stratum granulosum* and *stratum spinosum*, the *stratum basale* can be sometimes seen as a crisp, bright transition zone between highly scattering epidermis and less scattering papillary dermis (PD). The absence of melanocytes in the basal layer of epidermis and the undulations of the dermal papillae at the dermal–epidermal junction makes it hard to clearly demarcate the boundary between epidermis and dermis in glabrous skin. The PD is well demarcated from the reticular dermis (RD) by the *rete subpapillare* (RS), a dense network of capillaries at their relatively flat boundary. The PD, comprising fine collagen and elastin fibers and small blood vessels arising from the RS, seem to be a less scattering layer when compared to the RD, comprising large compact collagen fibers and thick elastin fibers.[61] At the region of the fold above the PIP joint, horizontal striations associated with lymphatic clefts and microvasculature can be seen deep inside the RD. Underneath the fibrous RD, structures resembling adipose fat conglomerations of the hypodermis can also be seen, before the intensity of backscattered light drops. Figure 1(c) shows a three-dimensional rendering constructed using 1024 B-scans obtained from the PIP joint of the middle finger and features a virtual dissection at the base of the SC and another one beneath the RS. Averaged *en face* views of the same volume sampled at different depths [Fig. 1(d)] unveil different morphological features more clearly due to the stratified nature of skin.

The fold above the PIP joint is an interesting region for obtaining OCT images of glabrous skin as it flattens out the undulations of dermal papillae, compacts underlying layers, and allows deeper penetration of light [Fig. 1(a)]. Figure 2 depicts cross-sectional and *en face* images of skin above the PIP joint obtained at three wavelengths. In this study, penetration depth appears to increase with wavelength at approximately identical locations, as demonstrated in many previous theoretical[52] and experimental[53,54] studies [Figs. 2(a)–2(c)]. Interestingly, even at 800 nm, it was possible to see structures as deep as the RD. *En face* views of different cutaneous layers were constructed by averaging in depth across 1024 B-scans within the range indicated by markers in the corresponding cross section [Figs. 2(d)–2(q)]. *En face* projections obtained at the main dermal layers demonstrate the wavelength-dependent appearance of different anatomical features. In the SC [Figs. 2(d)–2(f)], parallel ridges formed by the underlying dermal papillae can be clearly distinguished, on top of which sweat ducts, visible as bright spots, open [arrow in Fig. 2(d)]. The sweat ducts change their relative contrast and appear as dark spots inside the brighter islands formed by the highly scattering viable epidermis (VE) [Figs. 2(g)–2(i)] that is intersected by dark downward folds of thicker epidermis at dermal ridges. The PD [Figs. 2(j)–2(l)] can be easily recognized by its honeycomb-like structure formed by fibrous stroma of the RD around the comparatively less scattering darker base of the dermal papillae. The RD [Figs. 2(m)–2(q)] forms a high-scattering layer with a rich supply of blood vessels, which can be easily identified as signal-poor regions. The 1300-nm OCT system allowed better visualization of deeper structures of the RD, and no significant difference in contrast was noticed between the three wavelengths at this region of human skin.

In Fig. 3, images of hairy skin obtained from the dorsal forearm at three different wavelength regions are compared in terms of penetration depth and contrast. In the cross sections obtained by averaging three B-scans in order to reduce speckle, the various cutaneous sublayers along with their appendages are visualized as horizontal bands with remarkably different contrast. The increase in penetration depth with wavelength becomes more evident in hairy skin [Figs. 3(a)–3(c)]. Comparing the values of epidermal thickness obtained from the similar location in concurrent studies,[62,63] the bright narrow line on the surface of the cross-sectional images corresponds to the thin SC that is dominated by the highly scattering *stratum disjunctum*, followed by a lower scattering region of living epidermis and then a bright layer that corresponds to the *stratum basale* (SB) [arrow in Fig. 3(a)]. The SB appears as a highly scattering layer, making it more distinct in thin skin, due to the higher concentration of melanin-rich compartments in this portion of epidermis. This can also be seen in Fig. 4. The PD can be easily distinguished from the RD due to different scattering properties. Dark vertical lines in the cross-sectional images arise from the shadows cast by hair. Due to the higher average scattering in thin skin, a considerable difference in contrast was noticed between cutaneous layers depending on the wavelength used, with the 800-nm region offering better contrast over the other two wavelength regions. Figures 3(d)–3(f) show *en face* views of epidermis at 800 nm, 1060 nm, and 1300 nm, respectively. The fine grooves (*sulci cutis*) on the skin surface can be seen as a dark network, and the dermal ridge pattern on hairy skin is much less structured than in the glabrous skin. The PD can be clearly identified in the *en face* view, as it is characterized by dark portions of dermal papillae with intervening brighter portions of the RD [Figs. 3(g)–3(i)]. The RD appears as a dense fibrous layer with many blood vessels and skin appendages contributing to stronger scattering and absorption of incident light [Figs. 3(j)–3(n)]. The decay of signal intensity with depth on glabrous and hairy skin at different wavelength regions is compared in Fig. 4. The curves placed on the B-scans in Figs. 4(a) and 4(c) represent depth-dependent signal decay across two to three A-scans in the given cross sections at three different wavelength regions and depict the axial profile of the OCT signal, showing variations in backscattered intensity within different dermal layers. However, the curves in Figs. 4(b) and 4(d) were obtained by averaging A-scans

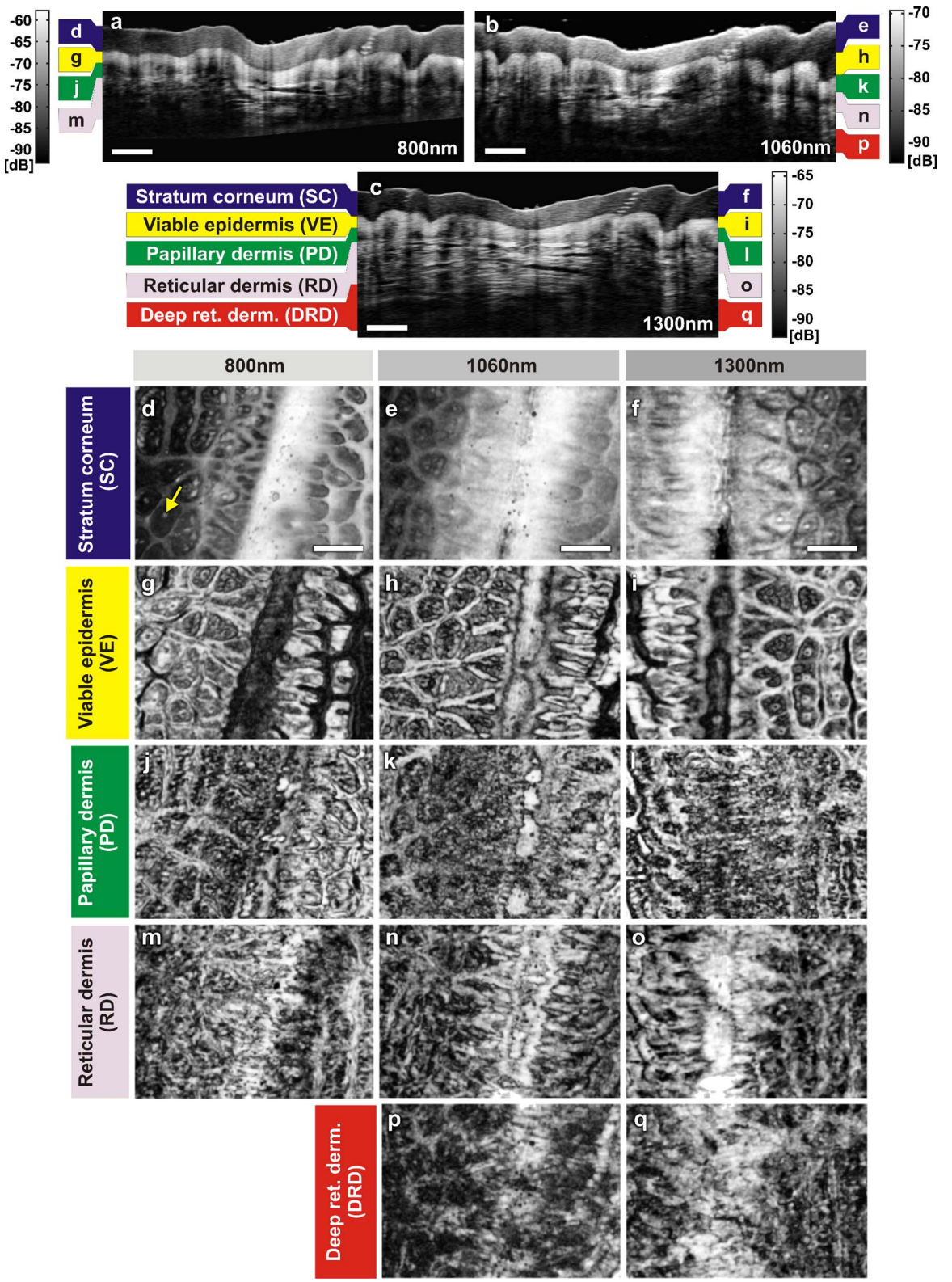

Fig. 2 Images of glabrous skin located above the proximal interphalangeal joint of the middle finger obtained using three OCT systems. B-scans obtained using (a) 800-nm, (b) 1060-nm, and (c) 1300-nm OCT systems. Dynamic ranges (dB) in these images are indicated using gray scales. *En face* images of various subsurface layers from 800-nm (d, g, j, m), 1060-nm (e, h, k, n, p), and 1300-nm (f, i, l, o, q) OCT systems. The yellow arrow in (d) denotes a sweat duct. The scale bars denote 500 μm in (a, b, c) and 1 mm in *en face* sections. (Color online only.)

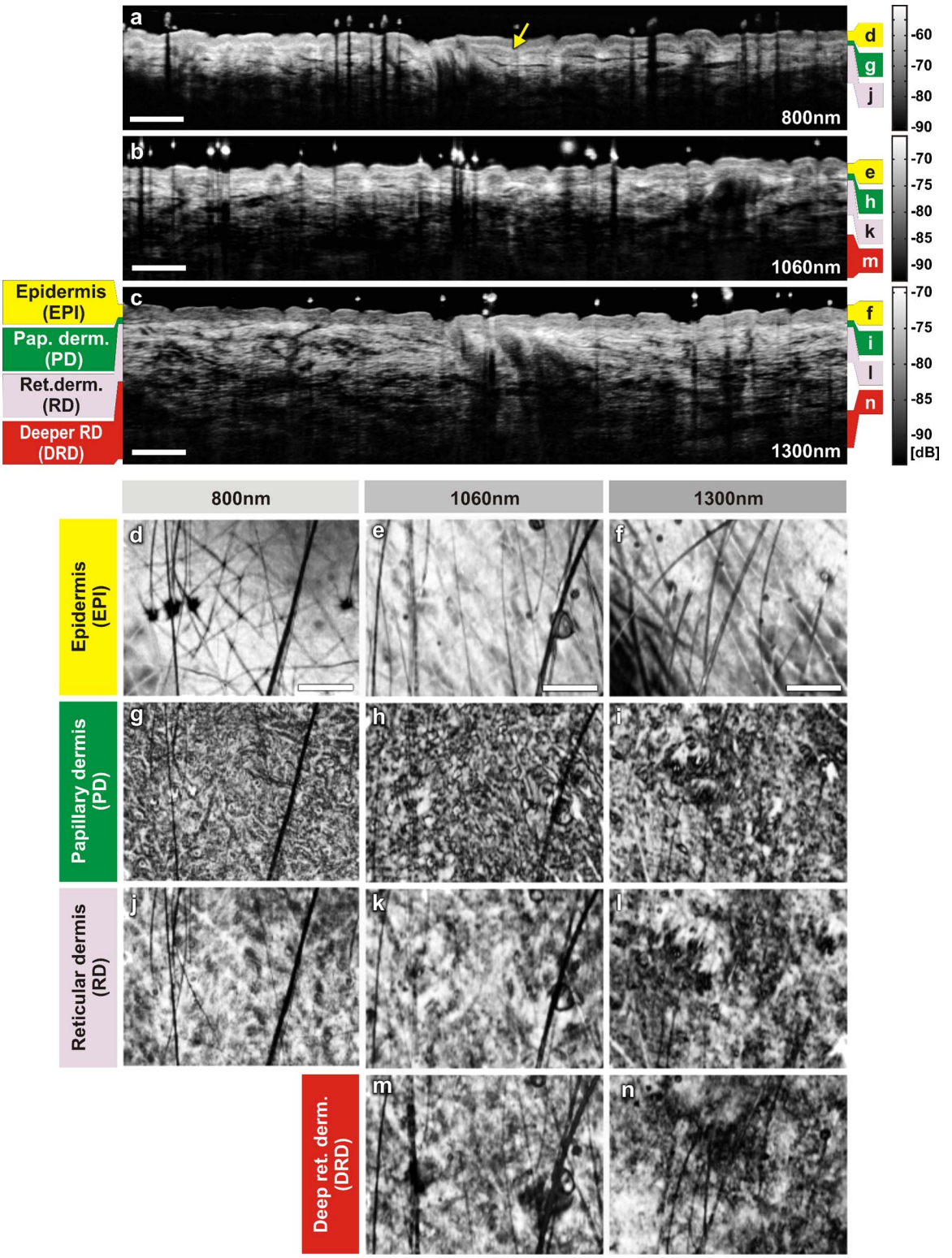

Fig. 3 Images of skin at the dorsal forearm obtained using three OCT systems. B-scans obtained using (a) 800-nm, (b) 1060-nm, and (c) 1300-nm OCT systems. Dynamic ranges (dB) in these images are indicated using gray scales. *En face* images of various subcutaneous layers from 800-nm (d, g, j,), 1060-nm (e, h, k, m), and 1300-nm (f, i, l, n) OCT systems. The scale bars denote 500 μm in (a, b, c) and 1 mm in *en face* sections.

across a volume stack of 200 B-scans at the same location, in order to emphasize the wavelength-dependent variation in the drop of signal intensity with depth, rather than the profile itself. The A-scan profiles show that the relative amplitude of signal intensity from various subcutaneous layers is slightly different depending on the wavelength region, and the averaged A-scan profiles confirm that the attenuation of OCT signal with depth is less at higher wavelength regions.

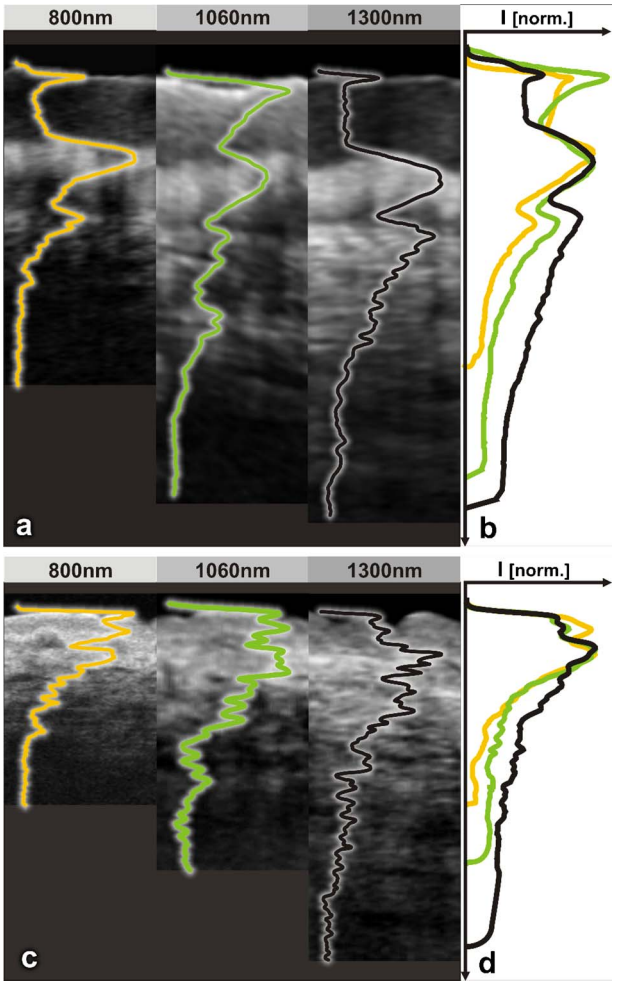

Fig. 4 Depth-dependent drop in signal intensity with wavelength in glabrous (a, b) and hairy (c, d) skin. A-scan profiles on glabrous skin (a) and hairy skin (c) at three different wavelengths. A-scan profiles averaged across a volume stack of 200 B-scans obtained from glabrous skin (b) and hairy skin (d).

In glabrous skin, eleidin functions as the primary UV-absorbent, rendering it white to pinkish in appearance regardless of skin phototype, while in hairy skin, melanin performs this function. Melanin is found in the form of highly scattering melanosomes, produced by the melanocytes, which are located at the SB. Melanin pigmentation of hairy skin influences light penetration at shorter wavelengths, and hence was postulated to affect the imaging depth of OCT by wavelength-dependent scattering and absorption. Figure 5 compares images of dorsal forearm skin taken from three different skin types (II, IV, and VI) at all three wavelengths, to determine the effect of skin pigmentation on OCT. (The visual appearance of the skin at the dorsal forearm of the three subjects imaged is indicated in the column labels.) As suggested in a previous study,[44] skin color does not appear to affect penetration depth in OCT within these set of samples, whereas the variation in depth of penetration with wavelength is quite evident in all the skin types, as shown in the Figs. 5(a)–5(i). Previous studies that attempted a comparison of skin types of various ethnic origins at a single wavelength[49] or using a multimodal approach[64] concluded that African-American (type VI) skin has more contrast at the dermal–epidermal junction and more prominent dermal papillae than Caucasian skin. In order to obtain more information about the anatomical differences between these three skin types, *en face* views were generated across 1024 B-scans at the basal layer of epidermis [Figs. 5(j)–5(r)]. The exact sampling location in depth is indicated by the markings to the right of each of the cross-sectional images. In these *en face* sections, a higher concentration of bright ring-shaped structures, known as "edged papillae," surrounding darker dermal papillae can be clearly seen in darker skin tones. The structural architecture of these edged papillae at the dermal–epidermal junction, critical in melanoma diagnosis, have been widely investigated using CLM.[65] The high resolution of the systems used in this study helped to identify the origin of higher contrast observed at the dermal–epidermal junction in darker skin types.

Figure 6(a) depicts the signal decay over depth in these three skin types at the 1300-nm region. The A-scan profiles show that the signal began to decay at a much faster rate in the RD when compared to the epidermis and the PD. As can be seen from the averaged A-scan profiles in Fig. 6(b), the OCT signal intensity first declined in the skin of the Caucasian subject, even when the epidermis of the African subject was thicker. The attenuation of light inside the tissue is influenced by both scattering and absorption, although the latter is much lower in the near-infrared region.[66] A previous study carried out to determine the absorption and reduced scattering coefficients of human skin in the wavelength range from 400 nm to 2000 nm concluded that the scattering at wavelengths larger than 600 nm originated from large Mie scatterers, such as collagen and elastin bundles.[67] This explains why the light penetration depth appeared to be independent of skin pigmentation, since the melanin, which behaves as a small Rayleigh scatterer, does not contribute significantly to the scattering of light in the wavelength regions employed for this study.

In addition to normal skin, a range of nevi and scar tissue was investigated to determine the changes in the structural organization of different skin layers, and also to analyze the performance of the three wavelength regions on different types of tissues. Figure 7 shows OCT images of a light-brown-colored intradermal nevus, which is characterized by cells that are confined within the dermis and is generally dome-shaped. As a result of the slightly different force applied by the handheld probe on the surface of nevus, its outer shape appears more or less flattened in B-mode scan cross sections obtained by the three OCT systems. As expected, the 1300-nm OCT system was capable of penetrating deeper into the nevus when compared to the other two systems [Figs. 7(a)–7(c)]. In the *en face* images of the upper dermis [Figs. 7(g)–7(i)], the dark structures postulated to be dilated blood vessels appear distinct from the brighter surroundings formed by the unaffected dermis. The 800-nm wavelength region provided a slightly better contrast over the other two wavelengths. OCT images of a black compound nevus, which is characterized by clusters of nevus cells present both in epidermis and dermis, are displayed in Fig. 8. The lower boundary of the nevus is able to be visualized only with the 1300-nm OCT system, as strong scattering by the densely packed nevus cells did not permit us to penetrate deep enough

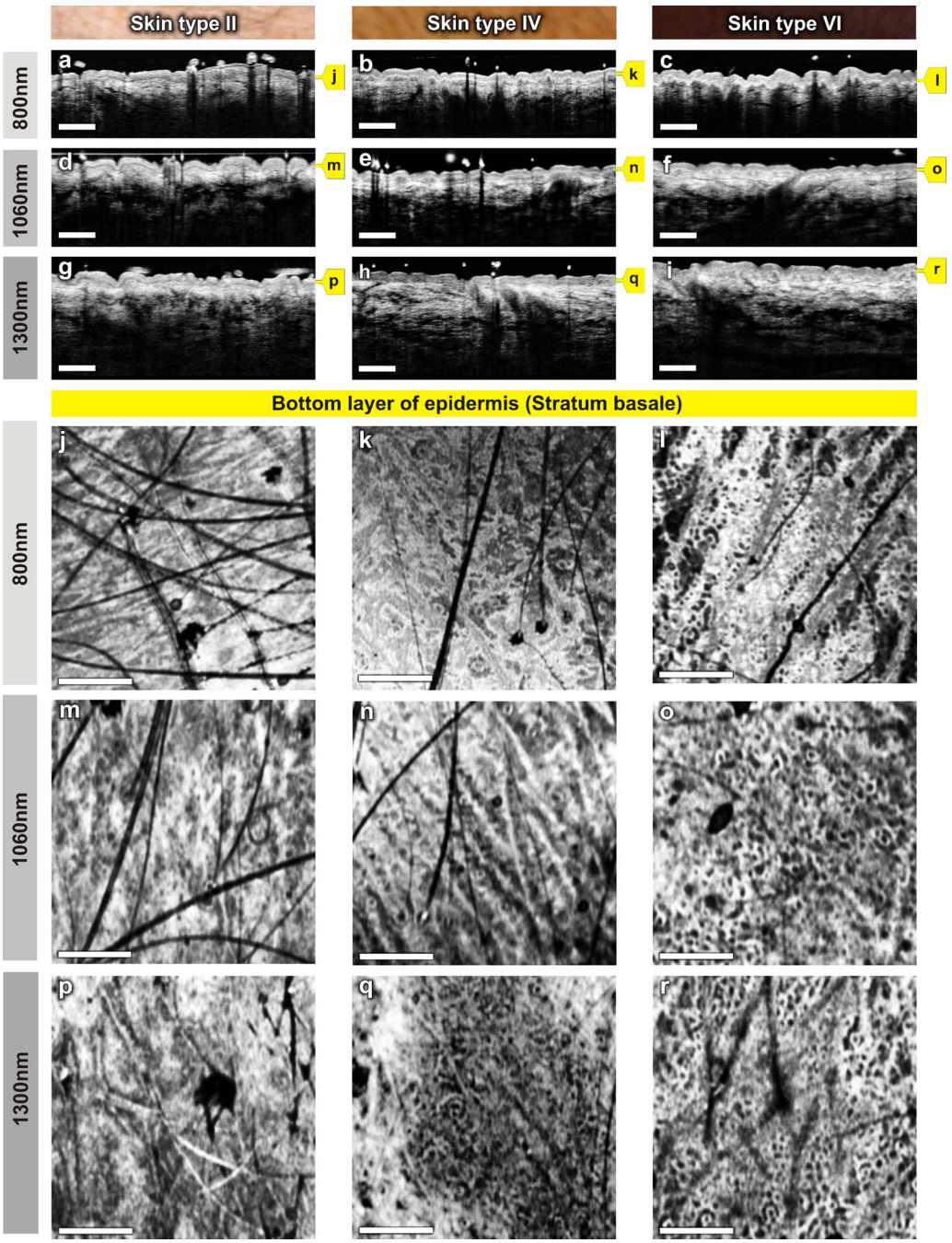

Fig. 5 Images of dorsal forearm skin taken using three OCT systems to show the effect of melanin pigmentation in OCT. B-scans of dorsal forearm skin comprising skin types II (Caucasian), IV (Indian), and VI (African) obtained using 800-nm (a, b, c), 1060-nm (d, e, f), and 1300-nm (g, h, i) OCT systems. *En face* images of the basal layer of the epidermis from these subjects obtained at 800 nm (j, k, l), 1060 nm (m, n, o), and 1300 nm (p, q, r). Edged papillae, comprising highly scattering melanin-rich keratinocytes, can be seen as bright rings surrounding the darker dermal papillae in the *en face* sections of the darker skin types. The scale bars denote 500 μm in cross sections and 1 mm in *en face* sections.

with shorter wavelength systems [Figs. 8(a)–8(c)]. However, the 800-nm system provided better contrast in the cross-sectional view, and the image contrast diminished for higher wavelengths. The surface area of the compound nevus can be determined from the *en face* views of epidermis [Figs. 8(d)–8(f)], and the decrease in strength of scattering with wavelength can be seen from the *en face* images of upper dermis [Figs. 8(g)–8(i)]. The deeper dermis (DD) region, directly underneath the nevus, becomes overcast by shadow in the *en face* image obtained at 800 nm, while more information is found at 1060 nm, and 1300 nm enables almost full reconstruction of the tissue underneath [Figs. 8(j)–8(l)].

Scars are areas of fibrous connective tissue that replace normal skin following an injury. They tend to be paler and denser than surrounding normal tissue due to a limited blood

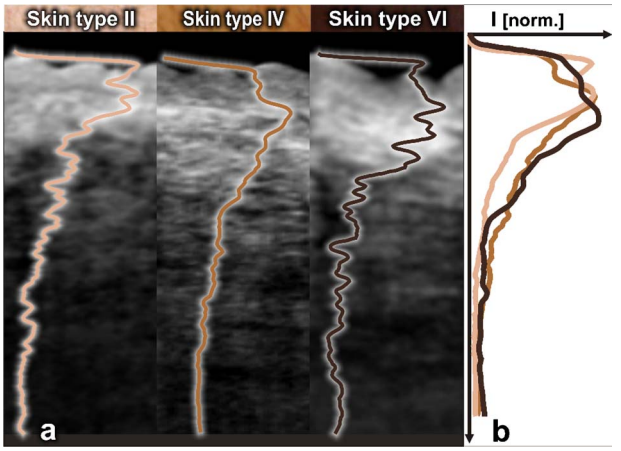

Fig. 6 Depth-dependent drop in signal intensity on skin above dorsal forearm among skin types II (Caucasian), IV (Indian), and VI (African). (a) A-scan profiles obtained at 1300 nm. (b) Average of A-scan profiles across a stack of 200 B-scans. These curves demonstrate that the skin pigmentation has little effect on light penetration.

supply. Scar tissues in skin are inferior to healthy skin due to loss of flexibility, reduced resistance to UV radiation, and incapability to grow sweat glands and hair follicles. As depicted in Fig. 9, in order to determine the nature and extent of structural deterioration in scar tissues, OCT images of a scar located above the PIP joint of the fourth finger were obtained at the three wavelength regions. The scar tissue appears as a dense brightly scattering region due to the higher collagen content. It lacks the layered structural arrangement found in the surrounding normal tissue as well as displays a notable thinning of the SC [boxes in Figs. 9(a)–9(c)]. The 1300-nm wavelength region was capable of penetrating deepest and allowed demarcation of the dimensions of the volume occupied by the scar tissue. *En face* views aided understanding of the pattern of scar formation and its variations in depth. The SC images [Figs. 9(d) and 9(e)] of this scar tissue indicate a different arrangement and density of sweat ducts, and the star-like shape of putative fibrous collagen content forming the scar seems to consist of lifted material from deeper layers [Figs. 9(g)–9(i)]. Again, images from the deeper RD obtained at 1300 nm allow investigation of the fine structure of the fibrous component that still forms a well-delineated region of higher density and deformation of the reticular meshwork, which cannot be extracted by the systems operating at lower wavelengths.

In this preliminary study, microstructural information obtained *in vivo* using OCT from different portions of the human skin was interpreted using textbook histology cross sections rather than the histology obtained from the excised tissue.[61] Morphological details were compared between identical regions of OCT scans only. This has advantages due to identical physical image generation principles in all images. However, this does not allow for identification of all structures and 1:1 correlation with gold standard histology. In this preliminary study, to find the effect of skin pigmentation on OCT, three subjects with distinctively different pigmentation levels were investigated, and no correlation was found between the depth of light penetration and skin pigmentation. Hence, this study supports the statement that the pigmentation has much lower influence on overall absorption and scattering in the near-infrared wavelength region than the surrounding tissue.[66,67] Although a larger number of subjects and locations might improve the quantification of an signal dependency on pigmentation, this result implies that it would be rather negligible. Another limitation of this study was the lack of an appropriate algorithm for segmenting different dermal layers. It should be possible to visualize different layers and their features much more distinctively through segmentation, less affected by their topology, to obtain more easily interpretable *en face* views.

The success of noninvasive treatment procedures using chemotherapeutic agents such as 5-flouroracil,[68] imiquimod,[69] and 5-aminolevulinic acid[70] in basal cell carcinomas and actinic keratoses emphasizes the need for noninvasive imaging modalities with adequate resolution and penetration depth for monitoring the disease progression. These noninvasive imaging techniques also help in delineating tumor margins, which is critical in surgery, photodynamic therapy, and radiotherapy of skin cancers. Among various dermal imaging modalities, OCT appears to be a promising methodology for investigating micromorphological and pathological features of human skin. Multiple studies have been performed to demonstrate the potential of OCT as a noninvasive tool for imaging skin tumors.[44,45,71] Critically sampled three-dimensional imaging capability, visualization of these volumes in arbitrary cross-sectional planes, and comparatively larger field of view obtained using OCT helps in detecting the tumor margins and other pathological conditions in lateral dimensions too.

A variety of noninvasive *in vivo* techniques showing promise as useful clinical tools in dermatology is currently being investigated. Imaging modalities with submicron-scale resolution, short acquisition time, sufficient contrast, adequate penetration depth, and good applicability are of particular importance. Skin structures down to a depth of 8 mm can be investigated using HFUS at 20 MHz, with a limited resolution of about 80 μm axially and 200 μm laterally.[26] HFUS is used in preoperative assessment and postoperative follow-up of skin tumors. CLM is one of the prominent noninvasive *in vivo* imaging modalities, which could perform optical sectioning of human skin in the horizontal plane with a resolution comparable to that of histology. However, the depth of imaging is limited to $\sim$300 μm at 830 nm due to tissue-induced aberrations and scattering.[23] This effect is also seen in the presented OCT images but has less influence on the OCT image formation. In CLM, imaging parameters such as field of view and axial and lateral resolutions are determined by the magnifying power and numerical aperture (NA) of the objective lens used. A routinely used objective lens with 30$\times$ magnification and 0.9 NA provides a field of view of 0.5 mm, a lateral resolution of 0.7 μm, and an optical section thickness of 3 μm at $\sim$30 Hz per individual cross section. To enable visualization of larger areas of tissue with varying magnification, a two-dimensional sequence of images can be captured and software-stitched into a mosaic.[23] However, this procedure does require a time-consuming repositioning of the focusing head. A comparative study using different illumination wavelengths (830 nm, 1064 nm, and 1100 nm) demonstrated that the depth of imaging increased to $\sim$350 μm at 1064 nm.[21] MPT is another emerging noninvasive imaging

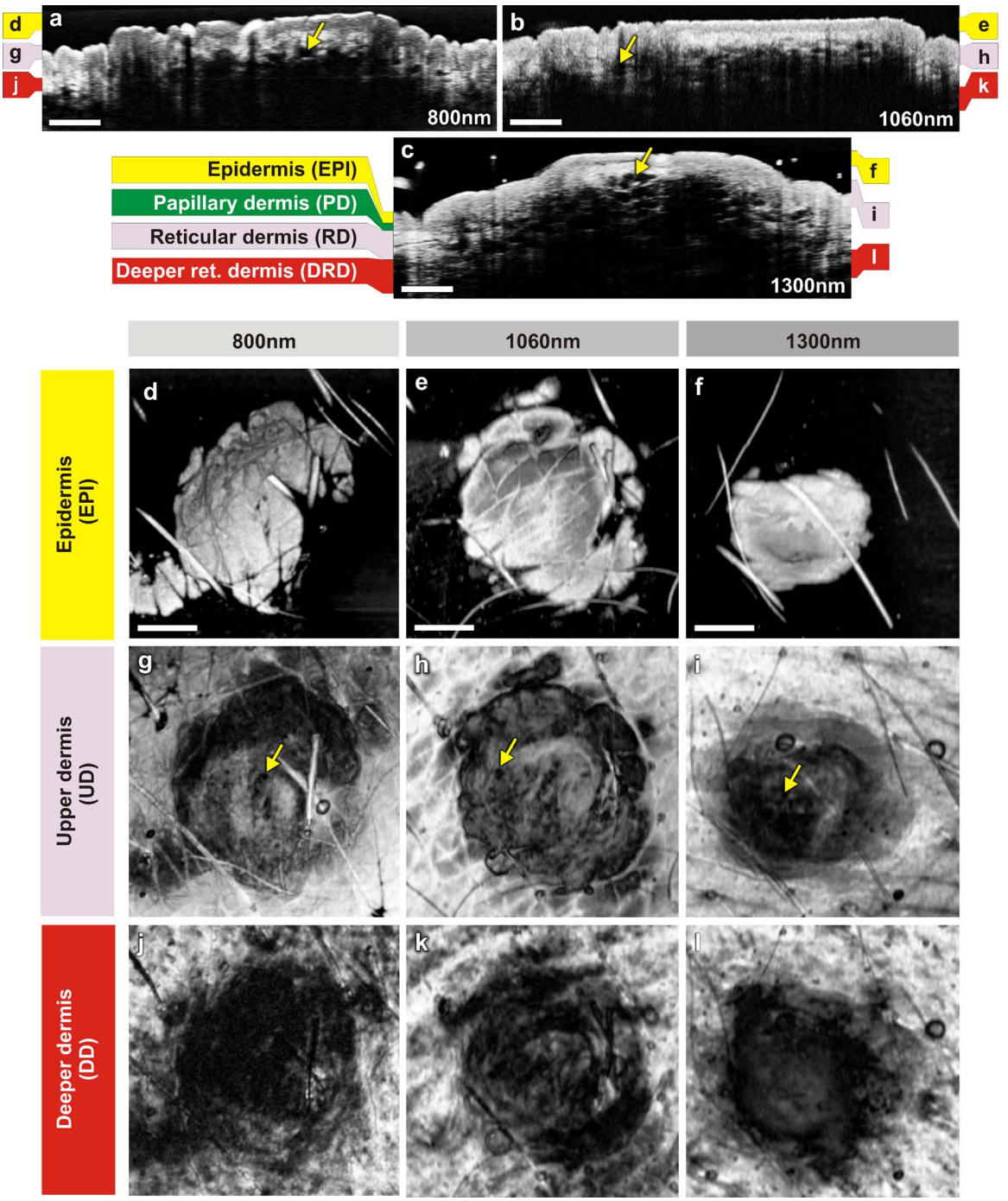

Fig. 7 Images of an intradermal nevus. B-scan of an intradermal nevus obtained using (a) 800-nm, (b) 1060-nm, and (c) 1300-nm OCT systems. *En face* views of different layers of intradermal nevus from 800-nm (d, g, j), 1060-nm (e, h, k), and 1300-nm (f, i, l) OCT systems. The dark structures, marked by yellow arrows, are postulated to be dilated blood vessels associated with the nevus. The scale bars denote 500 μm in cross sections and 1 mm in *en face* views. (Color online only.)

technique in which intense pulsed near-infrared laser beams (700 to 1000 nm) are focused onto a tiny excitation volume (1 μm^3) in order to realize nonlinear, nonconfocal high-resolution luminescence imaging. It enables 4-D functional imaging of subcellular structures as deep as $\sim$200 μm by detecting the second-harmonic signals, autofluorescence, and spatially resolved fluorescent decay kinetics. Typically, MPT offers a resolution of 250 ps temporally, 0.4 to 0.6 μm laterally, and 1.2 to 2 μm in the axial direction.[28] Although the resolution offered by OCT is superior to that of HFUS, it is inferior to that of MPT and CLM. Currently, depth of imaging seems to be most limited for MPT and CLM ($<$300 μm), followed by OCT (1 to 2 mm), and highest for HFUS ($\sim$8 mm at 20 MHz), among these dermal imaging techniques. All these imaging techniques are aiming to give access to huge data sets with the potential to give a complete repre-

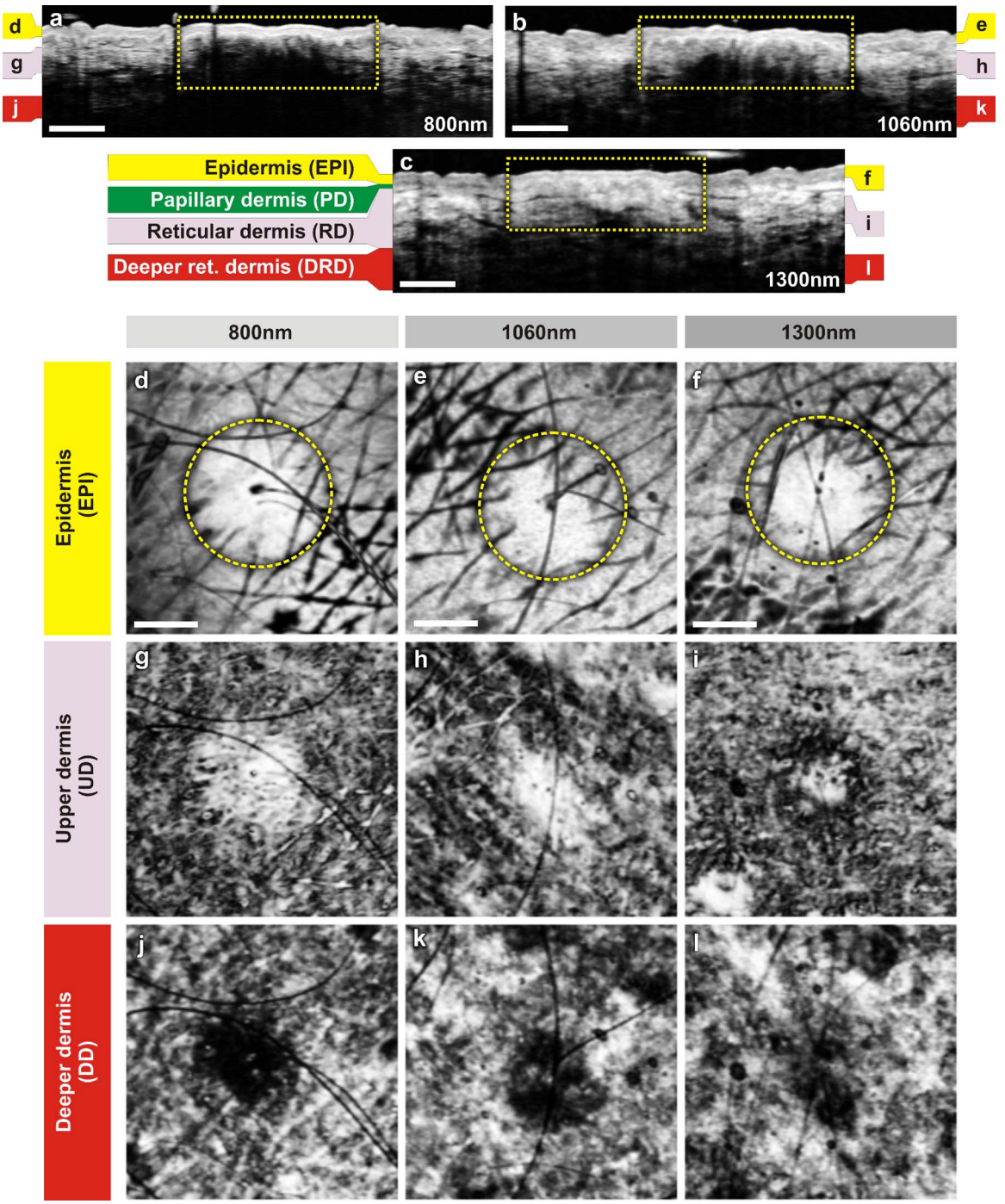

Fig. 8 Images of a compound nevus. B-scans of a compound nevus obtained using OCT at (a) 800 nm, (b) 1060 nm, and (c) 1300 nm. *En face* views of different layers of compound nevus obtained from 800-nm (d, g, j), 1060-nm (e, h, k), and 1300-nm (f, i, l) OCT systems. The scale bars denote 500 μm in cross sections and 1 mm in *en face* sections.

sentation of the morphology at the cellular level. For clinical applications, this raises the demand for automated detection of structural irregularities or more specific indicators typically based on spectroscopic information. While some of the competing techniques intrinsically deliver some kind of functional labeling, OCT in its current form is mainly limited to morphologic imaging. Consequently, it is indicated that only a combination of multiple noninvasive technologies will be able to replace all aspects of invasive histology with its ability for chemically selective high-resolution staining.

4 Conclusions

In this study, *in vivo* 3-D OCT images of human skin obtained at three different wavelength regions were compared in terms of resolution, penetration depth, and contrast. As expected, the

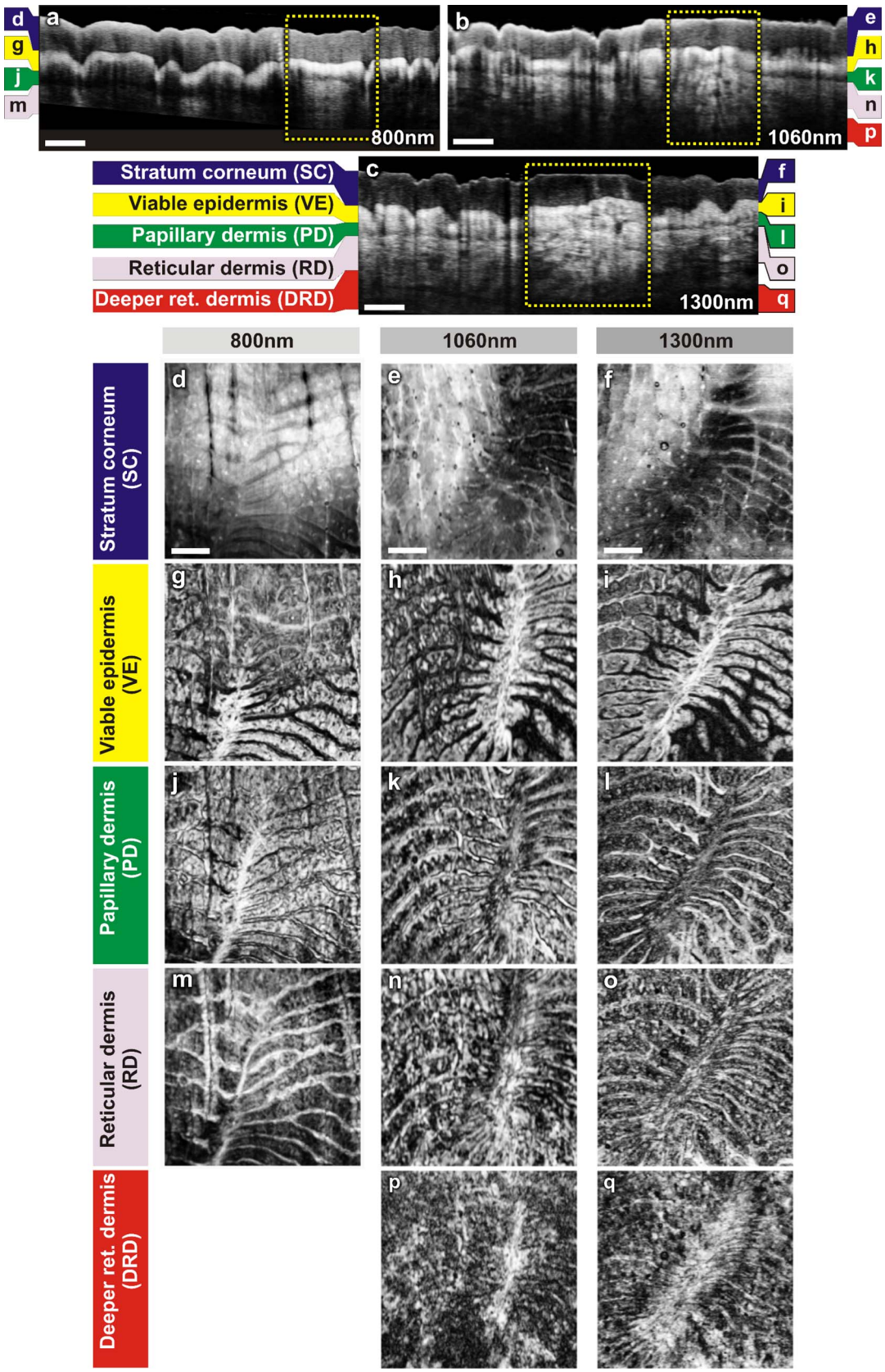

Fig. 9 Images of scar tissue on skin above the proximal interphalangeal joint of the fourth finger. B-scans of the scar obtained using (a) 800-nm, (b) 1060-nm, and (c) 1300-nm OCT systems. *En face* views sampled across different dermal layers obtained at 800 nm (d, g, j, m), 1060 nm (e, h, k, n, p), and 1300 nm (f, i, l, o, q) to illustrate increase in penetration depth with wavelength. The scale bars denote 500 μm in cross sections and 1 mm in *en face* sections.

longer wavelengths were less affected by scattering losses and were capable of deeper penetration. All major subepidermal layers along with their appendages were clearly visible to different depths using all the wavelength regions employed. Hairy and glabrous skin display a similar behavior at the highly scattering layers underneath the less scattering SC. Interestingly, scattering in the SC itself seems to be strongly dependent on wavelength, which leads to a very different appearance in both hairy and glabrous skin, especially at around 1 μm. The 800-nm system profits from the higher axial resolution, and also delivers higher contrast in comparison to 1300 nm. This could be primarily due the stronger scattering at smaller particles but also can be influenced by absorption due to endogenous chromophores such as melanin and hemoglobin. This study emphasizes the need for high axial resolution systems to enable discrimination of thin layers such as the SC ($\sim$20-μm thick) in hairy skin cross sections and also presents the advantage of high-speed imaging allowing high-resolution *en face* sections at different depths and thus enabling the differentiation of minute morphological structures and abnormalities.

In agreement with previous studies,[44] the investigation of normal subjects with different ethnic origins indicates that skin pigmentation does not affect the depth of light penetration, but rather demonstrates that the main amount of scattering at infrared wavelengths occurs in the dermis. Bright ring-shaped structures associated with highly scattering melanin-rich keratinocytes surrounding dermal papillae in darker skin tones could be demarcated within the basal layer of the epidermis and were found to locally increase the contrast at the dermal–epidermal junction. The investigation of moles and scar tissue during this study accentuated the need for employing higher wavelength sources to evoke information from deeper layers. Lower wavelength regions provided more contrast for superficial nevus nests in light-pigmented moles, while the nests of the thicker, highly pigmented moles were overcast by shadows, which could be suppressed by using longer wavelengths.

The dermal–epidermal junction, which is critical in early cancer diagnosis,[72] could be well delineated using the 800-nm system, and this wavelength is also best suited for pharmacological studies, which focus on the epidermal barrier function.[73,74] Meanwhile, employment of the 1300-nm wavelength region becomes inevitable in applications such as detection of deeper tumor margins, assessment of larger skin pathologies, and evaluation of treatment effects, which require information from deeper dermal layers. The 1060-nm region exhibits a performance between the 800-nm and 1300-nm wavelength regions in terms of penetration depth and contrast, but it is limited in axial resolution due to the reduced availability of ultra-broadband sources in this wavelength region. In summary, all three OCT systems have demonstrated their ability to acquire a gigavoxel image within $\sim$10 s with micron-scale resolution to varying imaging depths, thereby improving the scope for deploying this high-speed, high-resolution technology as a noninvasive method for diagnostics and treatment monitoring in dermatology.

Acknowledgments

This work was supported by the BBSRC, Wellcome Trust, Cardiff University, MRC, FP6-IST-NMP-2 STREPT (017128, NanoUB), DTI Grant (OMICRON), AMR Grant (AP1110), European Union Project FUN OCT (FP7 HEALTH, Contract No. 201880), MAXON Computer GmbH, and Carl Zeiss Meditec, Inc.

References

1. A. F. Fercher, K. Mengedoht, and W. Werner, "Eye-length measurement by interferometry with partially coherent light," *Opt. Lett.* **13**(3), 186–188 (1988).
2. D. Huang, E. A. Swanson, C. P. Lin, J. S. Schuman, W. G. Stinson, W. Chang, M. R. Hee, T. Flotte, K. Gregory, C. A. Puliafito, et al., "Optical coherence tomography," *Science* **254**(5035), 1178–1181 (1991).
3. W. Drexler and J. G. Fujimoto, *Optical Coherence Tomography: Technology and Applications*, Springer, Berlin (2008).
4. W. Drexler and J. G. Fujimoto, "State-of-the-art retinal optical coherence tomography," *Prog. Retin Eye Res.* **27**, 45–88 (2008).
5. A. Unterhuber, B. Považay, B. Hermann, H. Sattmann, W. Drexler, V. Yakovlev, G. Tempea, C. Schubert, E. M. Anger, P. K. Ahnelt, M. Stur, J. E. Morgan, A. Cowey, G. Jung, T. Le, and A. Stingl, "Compact, low-cost Ti:Al_2O_3 laser for *in vivo* ultrahigh-resolution optical coherence tomography," *Opt. Lett.* **28**(11), 905–907 (2003).
6. I. Hartl, X. D. Li, C. Chudoba, R. K. Ghanta, T. H. Ko, J. G. Fujimoto, J. K. Ranka, and R. S. Windeler, "Ultrahigh-resolution optical coherence tomography using continuum generation in an Ar-silica microstructure optical fiber," *Opt. Lett.* **26**(9), 608–610 (2001).
7. A. F. Fercher, C. K. Hitzenberger, G. Kamp, and S. Y. El-Zaiat, "Measurement of intraocular distances by backscattering speckle interferometry," *Opt. Commun.* **117**, 43–48 (1995).
8. W. Drexler, U. Morgner, F. X. Kartner, C. Pitris, S. A. Boppart, X. D. Li, E. P. Ippen, and J. G. Fujimoto, "*In vivo* ultrahigh-resolution optical coherence tomography," *Opt. Lett.* **24**(17), 1221–1223 (1999).
9. R. Leitgeb, C. K. Hitzenberger, and A. F. Fercher, "Performance of Fourier domain vs. time domain optical coherence tomography," *Opt. Express* **11**(8), 889–894 (2003).
10. J. F. de Boer, B. Cense, B. H. Park, M. C. Pierce, G. J. Tearney, and B. E. Bouma, "Improved signal-to-noise ratio in spectral-domain compared to time-domain optical coherence tomography," *Opt. Lett.* **28**(21), 2067–2069 (2003).
11. M. A. Choma, M. V. Sarunic, C. Yang, and J. A. Izatt, "Sensitivity advantage of swept source and Fourier domain optical coherence tomography," *Opt. Express* **11**(18), 2183–2189 (2003).
12. R. Huber, M. Wojtkowski, and J. G. Fujimoto, "Fourier domain mode locking (FDML): a new laser operating regime and applications for optical coherence tomography," *Opt. Express* **14**(8), 3225–3237 (2006).
13. B. Potsaid, I. Gorczynska, V. J. Srinivasan, Y. Chen, J. Jiang, A. Cable, and J. G. Fujimoto, "Ultrahigh speed spectral/Fourier domain OCT ophthalmic imaging at 70,000 to 312,500 axial scans per second," *Opt. Express* **16**(19), 15149–15169 (2008).
14. J. M. Olmedo, K. E. Warschaw, J. M. Schmitt, and D. L. Swanson, "Correlation of thickness of basal cell carcinoma by optical coherence tomography *in vivo* and routine histologic findings: a pilot study," *Dermatol. Surg.* **33**(4), 421–426 (2007).
15. T. Gambichler, G. Moussa, M. Sand, D. Sand, A. Orlikov, P. Altmeyer, and K. Hoffmann, "Correlation between clinical scoring of allergic patch test reactions and optical coherence tomography," *J. Biomed. Opt.* **10**(6), 064030–064035 (2005).
16. J. Welzel, M. Bruhns, and H. H. Wolff, "Optical coherence tomography in contact dermatitis and psoriasis," *Arch. Dermatol. Res.* **295**(2), 50–55 (2003).
17. A. Steiner, H. Pehamberger, and K. Wolff, "Improvement of the diagnostic accuracy in pigmented skin lesions by epiluminescent light microscopy," *Anticancer Res.* **7**(3B), 433–434 (1987).
18. G. Campos-do-Carmo and M. Ramos-e-Silva, "Dermoscopy: basic concepts," *Int. J. Dermatol.* **47**(7), 712–719 (2008).
19. G. Argenziano, G. Ferrara, S. Francione, K. D. Nola, A. Martino, and I. Zalaudek, "Dermoscopy—the ultimate tool for melanoma diagnosis," *Semin Cutan Med. Surg.* **28**(3), 142–148 (2009).
20. M. Rajadhyaksha, M. Grossman, D. Esterowitz, R. H. Webb, and R. R. Anderson, "*In vivo* confocal scanning laser microscopy of human skin: melanin provides strong contrast," *J. Invest. Dermatol.* **104**(6), 946–952 (1995).
21. M. Rajadhyaksha, S. González, J. M. Zavislan, R. R. Anderson, and

R. H. Webb, "*In vivo* confocal scanning laser microscopy of human skin II: advances in instrumentation and comparison with histology," *J. Invest. Dermatol.* **113**(3), 293–303 (1999).
22. A. Gerger, S. Koller, T. Kern, C. Massone, K. Steiger, E. Richtig, H. Kerl, and J. Smolle, "Diagnostic applicability of *in vivo* confocal laser scanning microscopy in melanocytic skin tumors," *J. Invest. Dermatol.* **124**(3), 493–498 (2005).
23. K. S. Nehal, D. Gareau, and M. Rajadhyaksha, "Skin imaging with reflectance confocal microscopy," *Semin Cutan Med. Surg.* **27**(1), 37–43 (2008).
24. K. Hoffmann, J. Jung, S. E. Gammal, and P. Altmeyer, "Malignant melanoma in 20-MHz B scan sonography," *Dermatology (Basel, Switz.)* **185**(1), 49–55 (1992).
25. S. E. Gammal, C. E. Gammal, K. Kaspar, C. Pieck, P. Altmeyer, M. Vogt, and H. Ermert, "Sonography of the skin at 100 MHz enables *in vivo* visualization of stratum corneum and viable epidermis in palmar skin and psoriatic plaquesy," *J. Invest. Dermatol.* **113**(5), 821–829 (1999).
26. M. H. Schmid-Wendtner, and D. Dill-Müller, "Ultrasound technology in dermatology," *Semin Cutan Med. Surg.* **27**(1), 44–51 (2008).
27. K. Konig and I. Riemann, "High-resolution multiphoton tomography of human skin with subcellular spatial resolution and picosecond time resolution," *J. Biomed. Opt.* **8**(3), 432–439 (2003).
28. K. König, "Clinical multiphoton tomography," *J. Biophoton.* **1**(1), 13–23 (2008).
29. E. Dimitrow, M. Ziemer, M. J. Koehler, J. Norgauer, K. Konig, P. Elsner, and M. Kaatz, "Sensitivity and specificity of multiphoton laser tomography for *in vivo* and *ex vivo* diagnosis of malignant melanoma," *J. Invest. Dermatol.* **129**(7), 1752–1758 (2009).
30. J. Bittoun, H. Saint-Jalmes, B. G. Querleux, L. Darrasse, O. Jolivet, I. Idy-Peretti, M. Wartski, S. B. Richard, and J. L. Leveque, "*In vivo* high-resolution MR imaging of the skin in a whole-body system at 1.5 T," *Radiology* **176**(2), 457–460 (1990).
31. S. Richard, B. Querleux, J. Bittoun, O. Jolivet, I. Idy-Peretti, O. de Lacharriere, and J.-L. Leveque, "Characterization of the skin *in vivo* by high resolution magnetic resonance imaging: water behavior and age-related effects," *J. Invest. Dermatol.* **100**(5), 705–709 (1993).
32. I. Rodríguez, S. Pérez-Rial, J. González-Jimenez, J. M. Pérez-Sánchez, F. Herranz, N. Beckmann, and J. Ruíz-Cabello, "Magnetic resonance methods and applications in pharmaceutical research," *J. Pharm. Sci.* **97**(9), 3637–3665 (2008).
33. J. Welzel, E. Lankenau, R. Birngruber, and R. Engelhardt, "Optical coherence tomography of the human skin," *J. Am. Acad. Dermatol.* **37**(6), 958–963 (1997).
34. J. Welzel, "Optical coherence tomography in dermatology: a review," *Skin Res. Technol.* **7**(1), 1–9 (2001).
35. T. Gambichler, G. Moussa, M. Sand, D. Sand, P. Altmeyer, and K. Hoffmann, "Applications of optical coherence tomography in dermatology," *J. Dermatol. Sci.* **40**(2), 85–94 (2005).
36. R. Steiner, K. Kunzi-Rapp, and K. Scharffetter-Kochanek, "Optical coherence tomography: clinical applications in dermatology," *Med. Laser Appl.* **18**(3), 249–259 (2003).
37. J. Welzel, E. Lankenau, G. Huttmann, and R. Birngruber, "OCT in dermatology," in *Optical Coherence Tomography: Technology and Applications*, W. Drexler and J. G. Fujimoto, Eds., ch. 35, pp. 1103–1121, Springer, Berlin (2008).
38. J. Strasswimmer, M. C. Pierce, B. H. Park, V. Neel, and J. F. de Boer, "Polarization-sensitive optical coherence tomography of invasive basal cell carcinoma," *J. Biomed. Opt.* **9**(2), 292–298 (2004).
39. S. M. Srinivas, J. F. de Boer, H. Park, K. Keikhanzadeh, H.-E. L. Huang, J. Zhang, W. Q. Jung, Z. Chen, and J. S. Nelson, "Determination of burn depth by polarization-sensitive optical coherence tomography," *J. Biomed. Opt.* **9**(1), 207–212 (2004).
40. M. C. Pierce, J. Strasswimmer, B. H. Park, B. Cense, and J. F. de Boer, "Birefringence measurements in human skin using polarization-sensitive optical coherence tomography," *J. Biomed. Opt.* **9**(2), 287–291 (2004).
41. Z. Chen, T. E. Milner, S. Srinivas, X. Wang, A. Malekafzali, M. J. C. van Gemert, and J. S. Nelson, "Noninvasive imaging of *in vivo* blood flow velocity using optical Doppler tomography," *Opt. Lett.* **22**(14), 1119–1121 (1997).
42. M. C. Pierce, J. Strasswimmer, B. H. Park, B. Cense, and J. F. de Boer, "Advances in optical coherence tomography imaging for dermatology," *J. Invest. Dermatol.* **123**(3), 458–463 (2004).
43. T. Gambichler, A. Orlikov, R. Vasa, G. Moussa, K. Hoffmann, M. Stücker, P. Altmeyer, and F. G. Bechara, "*In vivo* optical coherence tomography of basal cell carcinoma," *J. Dermatol. Sci.* **45**(3), 167–173 (2007).
44. M. Mogensen, B. M. Nürnberg, J. L. Forman, J. B. Thomsen, L. Thrane, and G. B. E. Jemec, "*In vivo* thickness measurement of basal cell carcinoma and actinic keratosis with optical coherence tomography and 20-MHz ultrasound," *Br. J. Dermatol.* **160**(5), 1026–1033 (2009).
45. T. Gambichler, P. Regeniter, F. G. Bechara, A. Orlikov, R. Vasa, G. Moussa, M. Stücker, P. Altmeyer, and K. Hoffmann, "Characterization of benign and malignant melanocytic skin lesions using optical coherence tomography *in vivo*," *J. Am. Acad. Dermatol.* **57**(4), 629–637 (2007).
46. N. D. Gladkova, G. A. Petrova, N. K. Nikulin, S. G. Radenska-Lopovok, L. B. Snopova, P. C. Yu, V. A. Nasonova, V. M. Gelikonov, G. V. Gelikonov, R. V. Kuranov, A. M. Sergeev, and F. I. Feldchtein, "*In vivo* optical coherence tomography imaging of human skin: norm and pathology," *Skin Res. Technol.* **6**(1), 6–16 (2000).
47. V. R. Korde, G. T. Bonnema, W. Xu, C. Krishnamurthy, J. Ranger-Moore, K. Saboda, L. D. Slayton, S. J. Salasche, J. A. Warneke, D. S. Alberts, and J. K. Barton, "Using optical coherence tomography to evaluate skin sun damage and precancer," *Lasers Surg. Med.* **39**(9), 687–695 (2007).
48. J. Welzel, C. Reinhardt, E. Lankenau, C. Winter, and H. H. Wolff, "Changes in function and morphology of normal human skin: evaluation using optical coherence tomography," *Br. J. Dermatol.* **150**(2), 220–225 (2004).
49. A. Pagnoni, A. Knuettel, P. Welker, M. Rist, T. Stoudemayer, L. Kolbe, I. Sadiq, and A. M. Kligman, "Optical coherence tomography in dermatology," *Skin Res. Technol.* **5**(2), 83–87 (1999).
50. M. A. Fox, G. D. Dayna, S. Karen, B. Adam, P. Tasneem, R. Allison, M. Massoud, and J. M. Roger, "Dermal scatter reduction in human skin: a method using controlled application of glycerol," *Lasers Surg. Med.* **41**(4), 251–255 (2009).
51. A. T. Yeh, B. Kao, W. G. Jung, Z. Chen, J. S. Nelson, and B. J. Tromberg, "Imaging wound healing using optical coherence tomography and multiphoton microscopy in an *in vitro* skin-equivalent tissue model," *J. Biomed. Opt.* **9**(2), 248–253 (2004).
52. A. W. Sainter, T. A. King, and M. R. Dickinson, "Effect of target biological tissue and choice of light source on penetration depth and resolution in optical coherence tomography," *J. Biomed. Opt.* **9**(1), 193–199 (2004).
53. Y. Pan and D. L. Farkas, "Noninvasive imaging of living human skin with dual-wavelength optical coherence tomography in two and three dimensions," *J. Biomed. Opt.* **3**(4), 446–455 (1998).
54. J. M. Schmitt, A. Knuttel, M. Yadlowsky, and M. A. Eckhaus, "Optical-coherence tomography of a dense tissue: statistics of attenuation and backscattering," *Phys. Med. Biol.* **39**(10), 1705–1720 (1994).
55. B. E. Bouma, L. E. Nelson, G. J. Tearney, D. J. Jones, M. E. Brezinski, and J. G. Fujimoto, "Optical coherence tomographic imaging of human tissue at 1.55 μm and 1.81 μm using Er- and Tm-doped fiber sources," *J. Biomed. Opt.* **3**(1), 76–79 (1998).
56. F. Spöler, S. Kray, P. Grychtol, B. Hermes, J. Bornemann, M. Först, and H. Kurz, "Simultaneous dual-band ultra-high resolution optical coherence tomography," *Opt. Express* **15**(17), 10832–10841 (2007).
57. S. Kray, F. Spöler, M. Först, and H. Kurz, "High-resolution simultaneous dual-band spectral domain optical coherence tomography," *Opt. Lett.* **34**(13), 1970–1972 (2009).
58. T. B. Fitzpatrick, "Soleil et peau," *J. Med. Esthetics* **2**, 33–34 (1975).
59. C. J. S. de Matos, S. V. Popov, and J. R. Taylor, "Temporal and noise characteristics of continuous-wave-pumped continuum generation in holey fibers around 1300 nm," *Appl. Phys. Lett.* **85**(14), 2706–2708 (2004).
60. B. Považay, B. Hermann, A. Unterhuber, B. Hofer, H. Sattmann, F. Zeiler, J. E. Morgan, C. Falkner-Radler, C. Glittenberg, S. Blinder, and W. Drexler, "Three-dimensional optical coherence tomography at 1050 nm versus 800 nm in retinal pathologies: enhanced performance and choroidal penetration in cataract patients," *J. Biomed. Opt.* **12**(4), 041211 (2007).
61. P. R. Wheater, J. W. Heath, and B. Young, "Skin," in *Wheater's Functional Histology: A Text and Colour Atlas*, ch. 9, pp. 157–171, Churchill Livingstone, London (2000).
62. J. Sandby-Møller, T. Poulsen, and H. C. Wulf, "Epidermal thickness at different body sites: relationship to age, gender, pigmentation,

blood content, skin type and smoking habits," *Acta Derm Venereol* **83**(6), 410–413 (2003).
63. T. Gambichler, R. Matip, G. Moussa, P. Altmeyer, and K. Hoffmann, "*In vivo* data of epidermal thickness evaluated by optical coherence tomography: effects of age, gender, skin type, and anatomic site," *J. Dermatol. Sci.* **44**(3), 145–152 (2006).
64. B. Querleux, T. Baldeweck, S. Diridollou, J. de Rigal, E. Huguet, F. Leroy, and V. H. Barbosa, "Skin from various ethnic origins and aging: an *in vivo* cross-sectional multimodality imaging study," *Skin Res. Technol.* **15**(3), 306–313 (2009).
65. G. Pellacani, A. M. Cesinaro, C. Longo, C. Grana, and S. Seidenari, "Microscopic *in vivo* description of cellular architecture of dermoscopic pigment network in nevi and melanomas," *Arch. Dermatol.* **141**(2), 147–154 (2005).
66. S. H. Tseng, P. Bargo, A. Durkin, and N. Kollias, "Chromophore concentrations, absorption, and scattering properties of human skin *in vivo*," *Opt. Express* **17**(17), 14599–14617 (2009).
67. A. N. Bashkatov, E. A. Genina, V. I. Kochubey, and V. V. Tuchin, "Optical properties of human skin, subcutaneous, and mucous tissues in the wavelength range from 400 to 2000 nm," *J. Phys. D* **38**(15), 2543–2555 (2005).
68. N. Krawtchenko, J. Roewert-Huber, M. Ulrich, I. Mann, W. Sterry, and E. Stockfleth, "A randomised study of topical 5% imiquimod vs. topical 5-fluorouracil vs. cryosurgery in immunocompetent patients with actinic keratoses: a comparison of clinical and histological outcomes including 1-year follow-up," *Br. J. Dermatol.* **157**(Suppl 2), 34–40 (2007).
69. C. Ulrich, J. O. Busch, T. Meyer, I. Nindl, T. Schmook, W. Sterry, and E. Stockfleth, "Successful treatment of multiple actinic keratoses in organ transplant patients with topical 5% imiquimod: a report of six cases," *Br. J. Dermatol.* **155**(2), 451–454 (2006).
70. N. McLoone, R. F. Donnelly, M. Walsh, O. M. Dolan, S. McLoone, K. McKenna, and P. A. McCarron, "Aminolaevulinic acid diffusion characteristics in *in vitro* normal human skin and actinic keratosis: implications for topical photodynamic therapy," *Photodermatol. Photoimmunol. Photomed.* **24**(4), 183–190 (2008).
71. J. K. Barton, K. W. Gossage, W. Xu, J. R. Ranger-Moore, K. Saboda, C. A. Brooks, L. D. Duckett, S. J. Salasche, J. A. Warneke, and D. S. Alberts, "Investigating sun-damaged skin and actinic keratosis with optical coherence tomography: a pilot study," *Technol. Cancer Res. Treat.* **2**(6), 525–535 (2003).
72. D. Komitowski, "Epidermal-dermal junction during experimental skin carcinogenesis and cocarcinogenesis as revealed by scanning electron microscopy," *J. Invest. Dermatol.* **78**(5), 395–401 (1982).
73. N. D. Barai, A. P. Supp, G. B. Kasting, M. O. Visscher, and S. T. Boyce, "Improvement of epidermal barrier properties in cultured skin substitutes after grafting onto athymic mice," *Skin Pharmacol. Physiol.* **20**(1), 21–28 (2007).
74. M. Gfesser, D. Abeck, J. Rügemer, V. Schreiner, F. Stäb, R. Disch, and J. Ring, "The early phase of epidermal barrier regeneration is faster in patients with atopic eczema," *Dermatology (Basel, Switz.)* **195**(4), 332–336 (1997).